Thermochimica Acta 489 (2009) 27–36

Contents lists available at ScienceDirect

Thermochimica Acta

journal homepage: www.elsevier.com/locate/tca

Thermal behavior of organotin(IV) triazolates: Molecular precursors for pure-phase, nanosized SnS/SnO_2

Mala Nath*, Sulaxna

Department of Chemistry, Indian Institute of Technology, Roorkee 247 667, India

ARTICLE INFO

Article history:
Received 24 July 2008
Received in revised form
26 December 2008
Accepted 1 January 2009
Available online 23 February 2009

Keywords:
Organotin(IV) triazolates
Thermogravimetric analysis
X-ray diffraction
Scanning electron microscopy
Transmission electron microscopy

ABSTRACT

The thermal behavior of organotin(IV) triazolates of general formula, R_nSnL_m ($n=3$, $m=1$; R = Me and Ph; $n=2$, $m=2$; R = Me and *n*-Bu; for HL = 4-amino-3-methyl-1,2,4-triazole-2-thiol (HL-**1**) and 4-amino-3-ethyl-1,2,4-triazole-2-thiol (HL-**2**); $n=2$, $m=2$, R = Ph for HL-**1**), has been investigated by thermogravimetry–differential thermal analysis–derivative thermogravimetric (TG–DTA–DTG) techniques. The thermal decomposition studies under air and nitrogen indicated different thermal behavior modes. This method provides a simple route to prepare nanosized (~6 to 60 nm) semiconductors SnS and SnO_2 in nitrogen and air atmosphere, respectively, at low temperature ~550 to 700 °C. The X-ray diffraction studies of the residues along with SEM and TEM measurements show that $Ph_2Sn(L\text{-}\mathbf{1})_2$ is the best precursor for pure-phase nanoscale SnO_2 and *n*-$Bu_2Sn(L\text{-}2)_2$ for SnS among the studied precursors, however, *n*-$Bu_2Sn(L\text{-}\mathbf{1})_2$ is a better precursor for the production of both nanoscale pure-phase SnO_2 and SnS.

1. Introduction

Thermal methods (TG/DTA/DTG) attracted a considerable attention of researchers during the last decade because of their wide spread practical application, especially, in the field of the production of nanoscale metallic particles/semiconducting metallic oxides or sulfides [1–5]. Moreover, thermogravimetric method provides a simple and cost effective route to prepare these nanoscale materials. Thermogravimetry and differential thermal analyses (TG/DTA) are not only the important tools in research and routine analysis, but also are valuable techniques for the study of the thermal properties of various compounds [1–9]. Organometallic compounds as single source precursors have attracted a great attention because they decompose at low temperatures producing pure metallic oxides/sulfides and metallic particles.

Semiconducting nanoparticles such as SnO_2 and SnS have been studied extensively owing to their potential applications in solar cells as transparent electrodes, photocatalysis and in optoelectronic industry [10–13], and used as gas sensors, heat mirrors, and varistors [14–17]. Especially, SnO_2 nanoparticles have been intensively studied for gas sensing applications not only because of their relatively low operating temperature, but also due to the fact that they can be used to detect both reducing and oxidizing gases. A variety of chemical and physical methods have been reported in the literature for the production of semiconducting nanoscale SnS [1,18–23] and SnO_2 [2,3,5,24–27]. In recent years, organotin–sulfur compounds have been explored as single source precursors for the preparation of semiconducting nanoscale SnO_2 and SnS [1–3,5]. Therefore, it is worth mentioning to explore further the best precursors, which can produce pure-phase, nanoscale SnS and SnO_2 on their pyrolysis.

In our research group, earlier studies relating to thermal behavior of a number of organotin compounds, and the preparation of tin(II) sulfide and tin(IV) oxide by pyrolysis of single source precursors have been reported [3,5,28–30] in order to explore the best precursors for the production of nanosized SnS and SnO_2, and also to improve the yield and the quality of tin-based materials. In continuation to our research interest, herein we report thermal decomposition of di-/triorganotin(IV) derivatives of 4-amino-3-methyl-1,2,4-triazole-2-thiol (HL-**1**) and 4-amino-3-ethyl-1,2,4-triazole-2-thiol (HL-**2**) in air and nitrogen by using TG and DTA techniques yielding semiconducting nanoscale SnO_2 and SnS. The particle size of the residues (SnO_2/SnS) obtained has been determined by X-ray diffraction analysis, SEM and TEM studies.

2. Experimental

2.1. Synthesis of di-/triorganotin(IV) derivatives of 4-amino-3-methyl-1,2,4-triazole-2-thiol (HL-**1**) and 4-amino-3-ethyl-1,2,4-triazole-2-thiol (HL-**2**)

Di-/triorganotin(IV) derivatives of 4-amino-3-methyl-1,2,4-triazole-2-thiol (HL-**1**) and 4-amino-3-ethyl-1,2,4-triazole-2-thiol

* Corresponding author. Tel.: +91 1332 285797; fax: +91 1332 273560.
E-mail address: malanfcy@iitr.ernet.in (M. Nath).

0040-6031/$ – see front matter © 2009 Elsevier B.V. All rights reserved.
doi:10.1016/j.tca.2009.01.019

(HL-**2**) have been synthesized according to previously reported method [31]. A methanolic solution (30 ml) of HL-**1**/HL-**2** (4.0 mmol) was added to sodium methoxide (prepared by dissolving sodium (4.2 mmol) in dry methanol (5 ml) under dry nitrogen. The reaction mixture was immediately turned to orange–red color, which was stirred for another 8 h at room temperature. To this, a methanol (30 ml) solution of R_2SnCl_2 (2.0 mmol)/R_3SnL (4.0 mmol) was added dropwise with constant stirring, and stirred for 30–35 h at room temperature. The reaction mixture was centrifuged and filtered in order to remove sodium chloride, and the volatiles were removed in vacuo. The solid obtained was recrystallized from methanol.

2.2. Measurements and characterizations

Thermogravimetric (TG) with simultaneous derivative thermogravimetric (DTG) and differential thermal analysis (DTA) of the organotin(IV) triazolates were performed on a PerkinElmer Pyris Diamond thermal analyzer. For TG analysis the weighed amount of the compound and reference (alumina powder) were placed in platinum crucibles of the pan sealed in a dry box. Samples of 10–15 mg were heated up to 1000 °C at a heating rate of 10 °C/min. Dry air and nitrogen gas were used as purge gases at a flow rate of 400 ml/min. The residues were prepared by the thermal decomposition of organotin(IV) precursors in a tube furnace under similar experimental conditions up to the formation temperature of SnS/SnO_2 as determined by TG. X-ray diffraction pattern (XRD) of the residues was recorded on the same instruments and under similar experimental conditions as reported previously [3,5]. The surface morphology of the residues was studied by using a scanning electron microscope (SEM) as reported previously [3,5] and by a transmission electron microscope (TEM). The TEM image of the residue obtained from pyrolysis of *n*-Bu_2Sn(L-**2**)$_2$ in air was recorded on a TEM model Philips, EM 400 at Institute Instrumentation Center, Indian Institute of Technology Roorkee, Roorkee and that obtained from *n*-Bu_2Sn(L-**1**)$_2$ in nitrogen was recorded on a TEM model Philips, Morgagni 268 D at Electron Microscopic Section, All India Institute of Medical Sciences, New Delhi. To record the SEM and TEM images of the residues the specimens were prepared according to the previously reported methods [3,5].

3. Results and discussion

The structure and stoichiometry of the single source precursors, organotin(IV) triazolates of general formula R_nSnL_m (n = 3, m = 1; R = Me and Ph; n = 2, m = 2; R = Me and *n*-Bu; for HL = 4-amino-3-methyl-1,2,4-triazole-2-thiol (HL-**1**) and 4-amino-3-ethyl-1,2,4-triazole-2-thiol (HL-**2**); n = 2, m = 2, R = Ph for HL-**1**), have been established by various physicochemical and spectral studies as reported in our previous communication [21], and are presented in Fig. 1(a) and (b).

The TG and DTA curves, respectively, of HL-**1** and HL-**2** in air, and their organotin(IV) derivatives in air and nitrogen, respectively, are presented in Figs. 2(a) and 3 and the results are given in Tables 1–4. DTG curves of a few compounds are also presented in Fig. 2(b). The XRD profiles of the residues obtained by thermal decomposition of organotin(IV) derivatives of HL-**1** and HL-**2** in both air and nitrogen atmosphere are presented in Figs. 4 and 5, respectively, and the main diffraction lines have been summarized in Table 5. The SEM images of the residue obtained from the pyrolysis of Ph_3Sn(L-**1**) in air, *n*-Bu_2Sn(L-**1**)$_2$ in nitrogen, *n*-Bu_2Sn(L-**2**)$_2$ in air and Ph_3Sn(L-**2**) in nitrogen are given in Fig. 6(a)–(d), and TEM images of the residues obtained by the pyrolysis of *n*-Bu_2Sn(L-**1**)$_2$ in nitrogen and *n*-Bu_2Sn(L-**2**)$_2$ in air are given in Fig. 7(a) and (b).

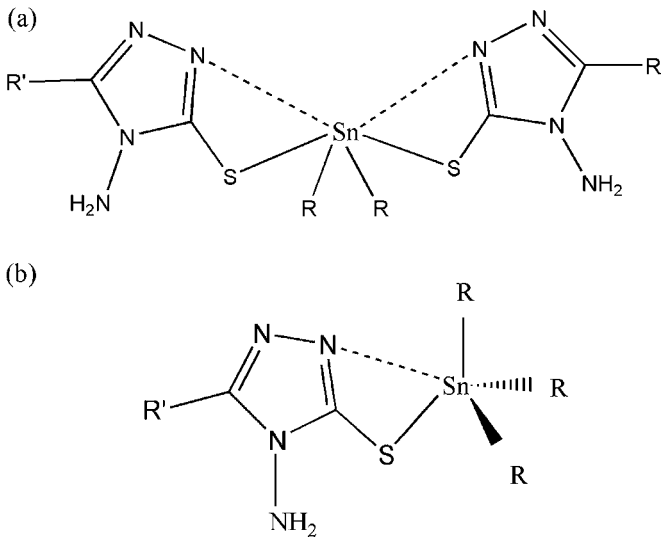

Fig. 1. Structure of R_2SnL_2 (where R = Me, *n*-Bu, *n*-Oct and Ph; HL = HL-**1** and HL-**2**) (a); and for R_3SnL (where R = Me, *n*-Pr, *n*-Bu and Ph; R′ = Me and Et; HL = HL-**1** and HL-**2**) (b).

3.1. Thermal decomposition of the ligands (HL-*1* and HL-*2*) under air

In air, HL-**1** and HL-**2** follow almost similar three steps decomposition pattern. Though the first decomposition step is not very clear from the TG profile of HL-**1**, but it is clearly defined by its DTG curve. This step corresponds to the loss of NH_2 (Tables 1 and 3) for both the ligands. However, the observed aggregate mass loss (for HL-**1**: 89.59%; for HL-**2**: 84.57%) in the second and third steps, corresponds to complete decomposition of the rest of organic moiety (Tables 1 and 3). The decomposition steps of the ligands under nitrogen are similar to those observed in air with only 1–2 °C difference in their weight loss step tangents.

3.2. Thermal decomposition of diorganotin(IV) triazolates under air and nitrogen

The TG plots of Me_2Sn(L-**1**)$_2$ exhibit complex and overlapping consecutive decomposition steps both in air and nitrogen. The mass loss observed in the first step corresponds to the loss of N_2H_4 in both air and nitrogen (Tables 1 and 2). Further, in air, the mass loss observed (obsd. 52.60%; calcd. 47.20%) in the second step corresponds to the loss of $C_8H_{12}N_6$ along with partial oxidation of tin, which is evidenced by the exothermic peaks observed at 468 and 590 °C in its DTA curve (Fig. 3). Thereafter, a very slow decomposition is continued up to 743 °C followed by rapid sublimation of the residue up to ~1000 °C (10.87% residue). The residue left at 1000 °C has been analyzed by powder XRD. The observed d values indicated a mixture of SnO_2 and SnO [32] (Table 5). However, in nitrogen, the second and third steps are overlapped; therefore, tentative temperature ranges have been assigned for these steps (Table 2). The weight loss observed in the second step corresponds to the loss of $C_6H_6N_6$ (obsd. 38.0%; calcd. 39.83%). The loss of C_2H_6S took place in the third step giving SnS which was completely sublimed up to 1000 °C. The XRD spectrum of the intermediate species formed at ~750 °C is not good, and the observed *d* values correspond mainly to those of SnS [32].

The first two steps of decomposition of Me_2Sn(L-**2**)$_2$ are same in both air and nitrogen (Tables 3 and 4) which correspond to the loss of N_2H_4 and $C_8H_{10}N_6$, respectively. The third weight loss step occurs in the temperature range 450–610 °C in air and 440–755 °C in nitrogen, and the observed mass losses are 12.60% and 11.14%,

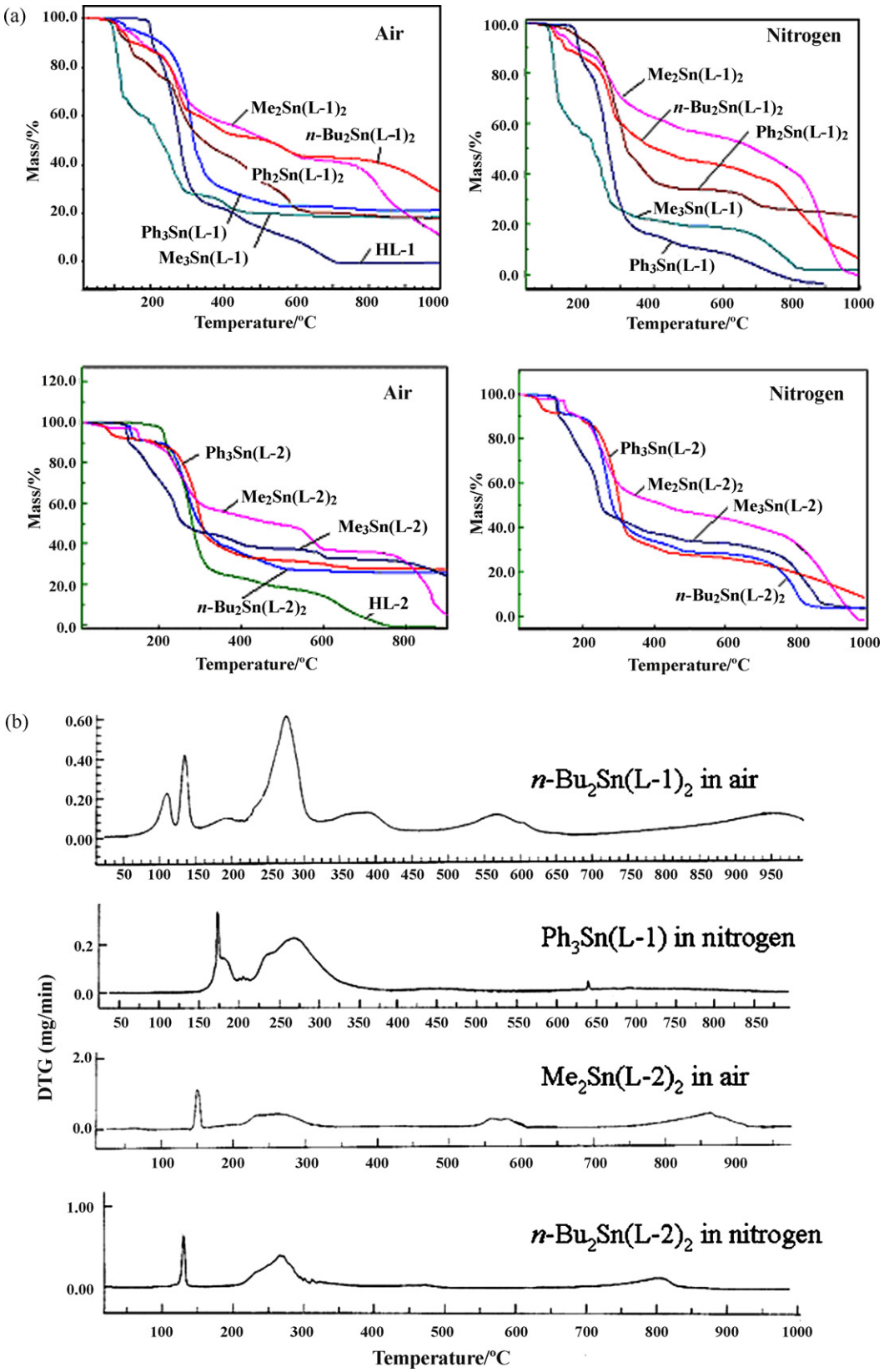

Fig. 2. (a) TGA plots of HL-**1**, HL-**2** in air, and their diorganotin(IV) triazolates and triorganotin(IV) triazolates under air and nitrogen. (b) DTG plots of *n*-Bu_2Sn(L-**1**)$_2$ and Me_2Sn(L-**2**)$_2$ under air and *n*-Bu_2Sn(L-**2**)$_2$ and Ph_3Sn(L-**1**) under nitrogen.

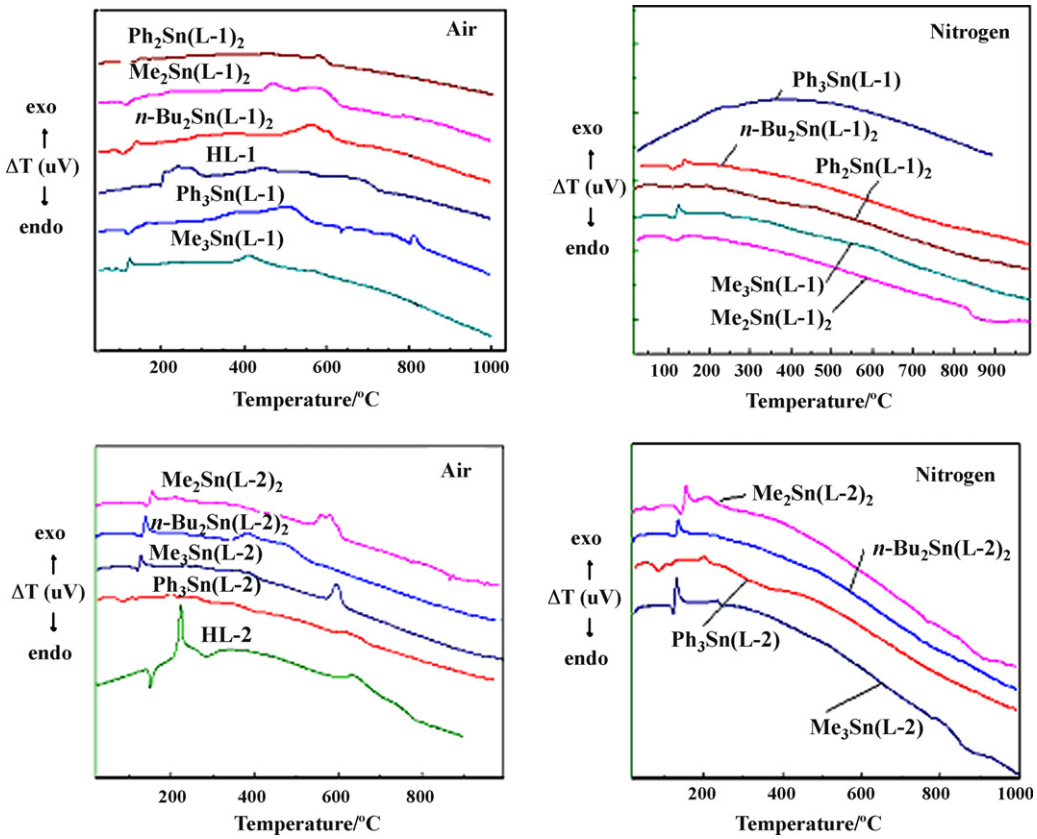

Fig. 3. DTA plots of HL-**1**, HL-**2** in air, and their diorganotin(IV) and triorganotin(IV) triazolates under air and nitrogen.

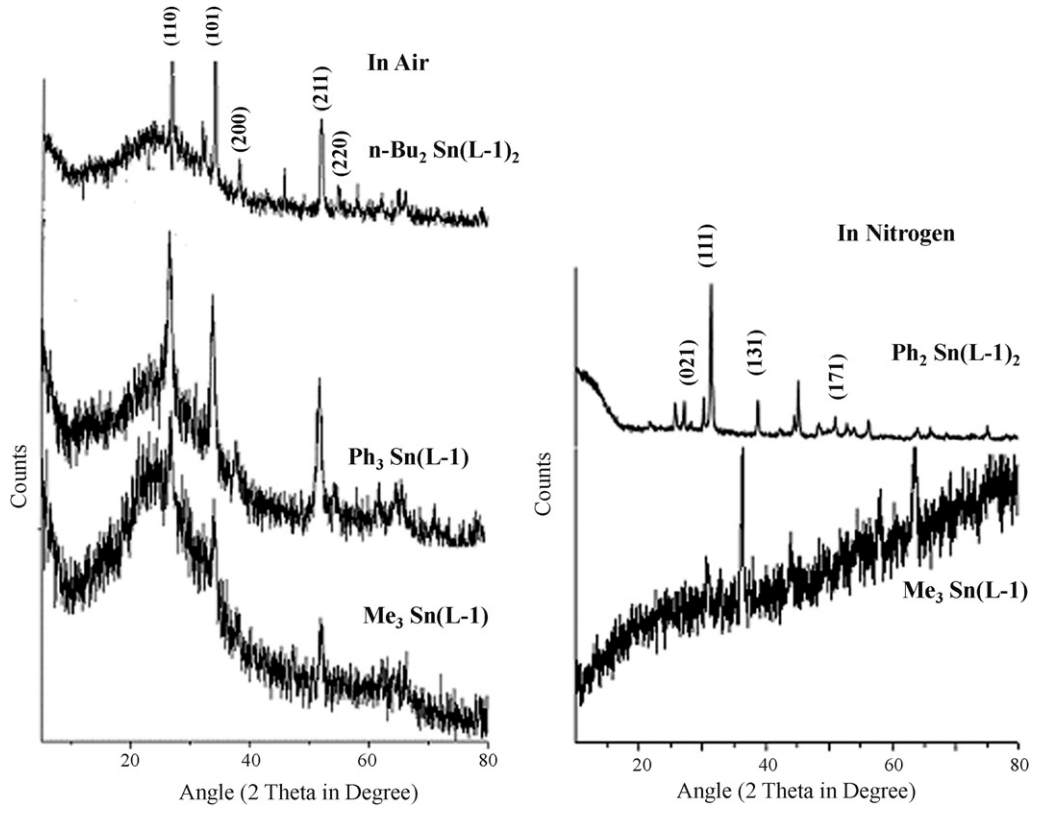

Fig. 4. XRD patterns of the residues obtained by the thermal decomposition of di- and triorganotin(IV) derivatives of HL-**1** under air and nitrogen.

Table 1
Thermal analysis data of 4-amino-3-methyl-1,2,4-triazole-2-thione (HL-**1**) and its organotin(IV) derivatives in air.

Ligand/compound	Step	$T_{range\,TG}$ (°C)	$T_{peak\,DTG}$ (°C)	$T_{peak\,DTA}$ (°C) (enthalpy mJ/mg)	Loss of mass%	
					Obsd. (calcd.)	Species lost
HL-**1**	I	188–205	203	209	10.41 (12.31)	NH_2
	II	205–333	277	238 (−1094)	63.46	Rest of the ring moiety
				272		
	III	333–725	443[a]	447 (−69)	26.13 (87.69)	
			670[a]	672 (−566)		
Me_2Sn(L-**1**)$_2$	I	80–177	114	117 (136)	10.46 (7.88)	N_2H_4
			174			
	II	177–618	269	197 (14)	46.69 (47.21)	$C_8H_{12}N_6$
			461	468 (−222)		
			588	590 (−648)		
	III	618–1000	830	785 (−60)	31.98 (15.76)	2S and Sublimation
n-Bu_2Sn(L-**1**)$_2$	I	82–115	108	110 (87)	5.66 (6.52)	N_2H_4
	II	115–150	135	140 (−82)	5.58 (6.12)	C_2H_6
	III	150–299	274	Broad exotherm	26.26 (26.88)	C_4N_6
	IV	299–405	378	Broad exotherm	9.12 (11.63)	C_4H_9
	V	405–608	566	561 (−784)	9.45 (11.63)	C_4H_9
	VI	608–979	947	Broad exotherm	13.47 (13.06)	2S
Ph_2Sn(L-**1**)$_2$	I	88–132	109	110 (171)	8.80 (6.04)	N_2H_4
	II	132–155	147	151 (−102)	6.51 (5.66)	C_2H_6
	III	155–255	209	Broad exotherm	11.46 (12.43)	C_2N_3
	IV	255–605	259	455 (−235)	51.35 (53.53)	$C_{14}H_{10}N_3S_2$
			278	600 (−504)		
			583			
Me_3Sn(L-**1**)	I	71–134	107	110 (139)	33.21 (33.14)	$C_3H_5N_4$
			118	123 (−63)		
	II	134–299	209	Broad exotherm	37.95 (26.34)	C_3H_9S
			251			
	III	299–455	408	413 (−369)	7.94 (−)	Sublimation
Ph_3Sn(L-**1**)	I	85–539	130	117 (81)	76.24 (75.22)	All organic moieties attached to tin
			313	168 (−40)		
			343	365 (−113)		
				512 (−602)		

[a] Very small peak.

respectively (calcd. 14.28% for loss of C_2H_6S), yielding an intermediate. This intermediate sublimed in the temperature range 717–907 °C in air and 755–970 °C in nitrogen. Only 4.4% residue was left at 984 °C in air. The XRD analysis (Table 5) of the residue formed at 610 °C in air indicated the formation of SnO_2, whereas the main diffraction lines obtained in the XRD pattern of the intermediate species formed at 755 °C in nitrogen indicated the formation of SnS [32].

Table 2
Thermal analysis data of organotin(IV) derivatives of 4-amino-3-methyl-1,2,4-triazole-2-thione (HL-**1**) in nitrogen.

Compound	Step	$T_{range\,TG}$ (°C)	$T_{peak\,DTG}$ (°C)	$T_{peak\,DTA}$ (°C) (enthalpy mJ/mg)	Loss of mass%	
					Obsd. (calcd.)	Species lost
Me_2Sn(L-**1**)$_2$	I	92–163	116, 154	118 (120)	9.0 (7.88)	N_2H_4
	II	163–637	275, 454	–	38.0 (39.83)	$C_6H_6N_6$
	III	637–828	–	–	14.0 (15.26)	C_2H_6S
	IV	828–1000	894	888 (591)	39.0 (37.03)	Sublimation
n-Bu_2Sn(L-**1**)$_2$	I	90–118	110	111 (79)	6.0 (6.52)	N_2H_4
	II	118–150	136	139 (−75)	6.0 (6.12)	C_2H_6
	III	150–583	187, 272	Broad exotherm	44.0 (50.14)	$C_8H_{18}N_6$
	IV	583–750	–	Broad exotherm	8.0 (6.53)	Oxidation of S
	V	750–995	835	Broad exotherm	29.0 (−)	Sublimation
Ph_2Sn(L-**1**)$_2$	I	133–439	175, 282 311, 371	111 (14)[a]	65.0 (65.58)	All organic moieties
				212 (17)[a]		
	II	439–725	680	460 (−78)[b]	8.0 (6.04)	Oxidation of S
Me_3Sn(L-**1**)	I	85–125	109, 118	112 (48)[a]	34.0 (33.14)	$C_3H_5N_4$
				123 (−74)[b]		
	II	125–276	170, 219 248	Broad exotherm	38.0 (15.39)	$3CH_3$ + sublimation
	III	276–819	–	Broad exotherm	26.0 (−)[b]	Sublimation
Ph_3Sn(L-**1**)	I	160–370	175, 270	Broad exotherm	85.0 (75.23)	All organic moieties attached to tin
	II	370–760	439[a], 636[a]	Broad exotherm	15.0 (−)[b]	Sublimation

[a] Very small peak.
[b] Unidentified mass loss.

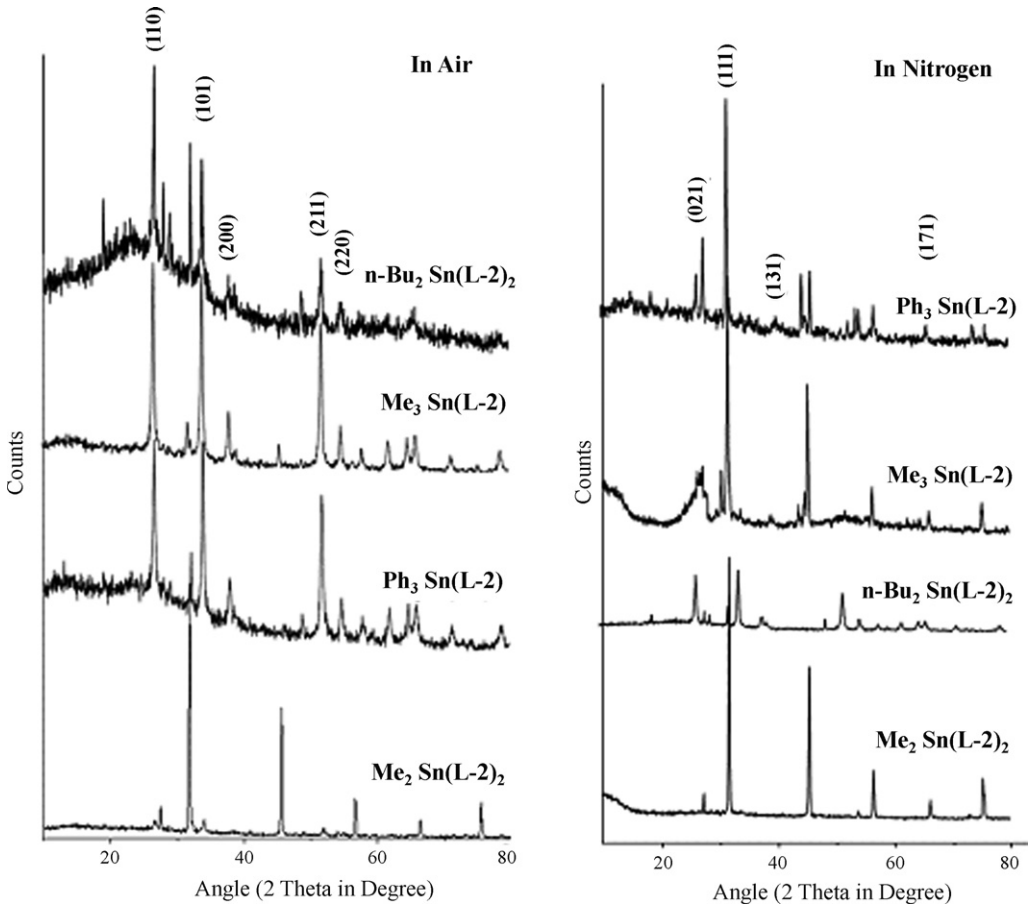

Fig. 5. XRD patterns of the residues obtained by thermal decomposition of di- and triorganotin(IV) derivatives of HL-**2** under air and nitrogen.

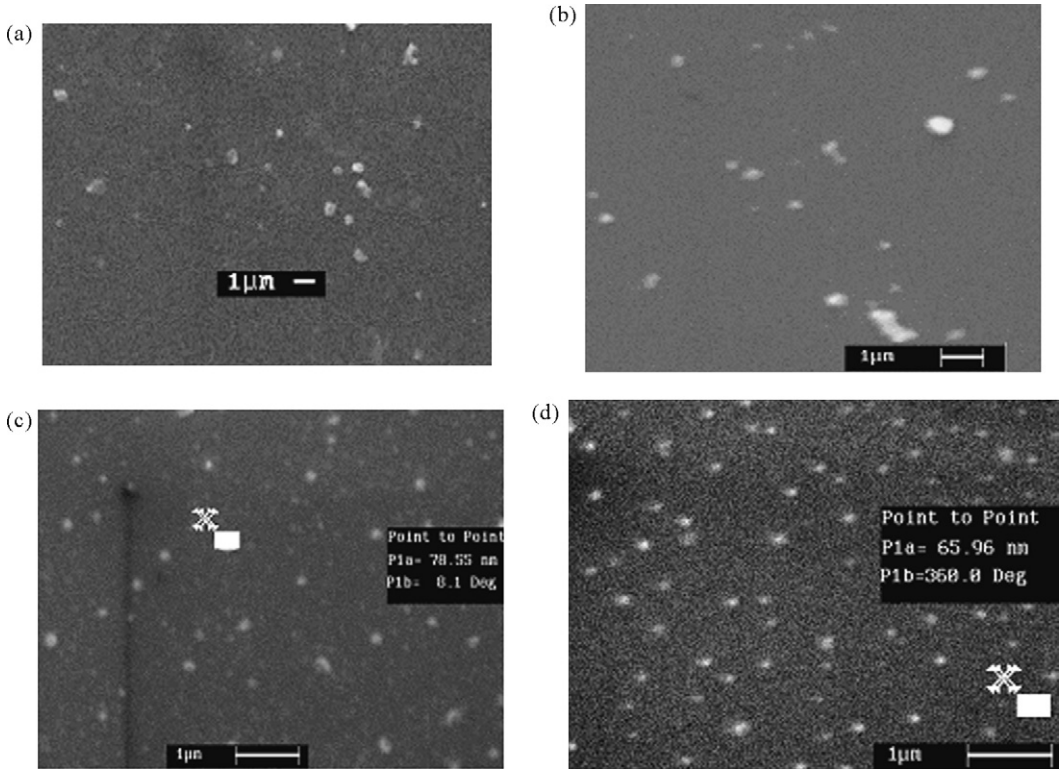

Fig. 6. SEM image of residues obtained by thermal decomposition of Ph_3Sn(L-**1**) in air (a); *n*-Bu_2Sn(L-**1**)$_2$ in nitrogen (b); *n*-Bu_2Sn(L-**2**)$_2$ in air (c); and Ph_3Sn(L-**2**) in nitrogen (d).

Table 3
Thermal analysis data of 4-amino-3-ethyl-1,2,4-triazole-2-thione (HL-**2**) and its organotin(IV) derivatives in air.

Compound	Step	$T_{range\,TG}$ (°C)	$T_{peak\,DTG}$ (°C)	$T_{peak\,DTA}$ (°C) (enthalpy mJ/mg)	Loss of mass%	
					Obsd. (calcd.)	Species lost
HL-**2**	I	145–226	218	150 (153) 223(−331)	15.43 (11.11)	NH_2
	II	226–342	280	279 (101)	58.53	Rest of the organic moiety
	III	342–771	650[a]	635 (−262) 744 (−56)	26.04 (88.89)	
Me_2Sn(L-**2**)$_2$	I	140–155	150	140 (80)	8.30 (7.36)	N_2H_4
	II	155–450	256	155 (−50) 209 (−70)	42.80 (43.73)	$C_8H_{10}N_6$
	III	450–610	559, 581	581 (−514)	12.60 (14.28)	C_2H_6S
	IV	717–907	858	773 (13) 864 (39)	31.90 (−)[b]	Sublimation
n-Bu_2Sn(L-**2**)$_2$	I	120–142	134	130 (74) 139 (−96)	8.50 (6.17)	N_2H_4
	II	142–560	272 353	226 (−64) 362 (−1164) 474	65.70 (71.0)	Rest of the organic groups attached to tin
Me_3Sn(L-**2**)	I	113–130	124	121 (28) 127 (−69)	10.50 (5.22)	NH_2
	II	130–291	243	235 (−12) 260 (−25)	43.10 (45.68)	$C_7H_{14}N_3$
	III	291–548	385	378 (−108)	9.40 (10.45)	Oxidation
	IV	548–993	597	593 (−332)	18.90 (−)[b]	Oxidation and sublimation
Ph_3Sn(L-**2**)	I	59–90	80	84 (68)	8.0 (9.14)	C_2H_7N
	II	90–418	195, 303	117 (10) 200 (−35) 254 (−56) 308 (−5) 346 (−71)	58.60 (60.28)	$C_{20}H_{15}N_3$
	III	418–660	585[a]	617 (−169)	5.0 (6.50)	Oxidation

[a] Small and broad peak.
[b] Unidentified mass loss.

n-Bu_2Sn(L-**1**)$_2$ exhibited a complex decomposition profiles both in air and nitrogen (Tables 1 and 2). The first two steps are similar in both atmospheres and the observed mass losses in these steps correspond to the loss of N_2H_4 and C_2H_6, respectively. However, the mass loss observed in the third step corresponds to the loss of C_4N_6 in air and $C_8H_{18}N_6$ in nitrogen. The third step in air is overlapped by fourth and fifth steps, followed by oxidation, leaving a residue of 30.46% (calcd. for SnO_2: 30.26%) at 979 °C, which is confirmed as SnO_2 by its XRD spectrum (Table 5). Whereas, in nitrogen, the fourth mass loss step in the temperature range 583–750 °C is overlapped

Table 4
Thermal analysis data of organotin(IV) derivatives of 4-amino-3-ethyl-1,2,4-triazole-2-thione (HL-**2**) in nitrogen.

Compound	Step	$T_{range\,TG}$ (°C)	$T_{peak\,DTG}$ (°C)	$T_{peak\,DTA}$ (°C) (enthalpy mJ/mg)	Loss of mass%	
					Obsd. (calcd.)	Species lost
Me_2Sn(L-**2**)$_2$	I	135–157	151	140 (56) 155 (−68)	8.02 (7.36)	N_2H_4
	II	157–440	267	210 (−82)	43.98 (43.73)	($C_8H_{10}N_6$)
	III	440–755	–	Broad exotherm	11.14 (14.28)	C_2H_6S
	IV	755–970	–	768 (9)	36.80 (−)[a]	Sublimation
n-Bu_2Sn(L-**2**)$_2$	I	115–136	132	125 (60) 134 (−103)	8.20 (6.17)	N_2H_4
	II	136–490	272 473[b]	–	62.70 (64.82)	Rest of the organic moiety
	III	490–830	802	–	25.20 (−)[a]	Sublimation
Me_3Sn(L-**2**)	I	123–131	127	123 (42)	9.10 (5.22)	NH_2
	II	131–295	242	131 (−92) 235 (−16) 247 (11)	48.1 (45.68)	$C_7H_{14}N_3$
	III	295–880	861	871 (250)	39.40 (−)[a]	Sublimation
Ph_3Sn(L-**2**)	I	57–98	82	85 (76)	9.0 (9.14)	C_2H_7N
	II	98–452	197 306	116 (10) 200 (−31)	62.50 (60.28)	$C_{20}H_{15}N_3$
	III	452–993	–	–	20.20 (−)[a]	Sublimation

[a] Unidentified mass loss.
[b] Very small peak.

Table 5
The main diffraction lines (intensity) and crystal average size calculated by Scherrer equation for the residue obtained in air and nitrogen atmosphere.

Residue of precursors	Main diffraction lines *d*, Å (intensity %) (*h k l*)					Average size *D* (nm)
	1	2	3	4	5	
Sn[a]	2.92 (100) (2 0 0)	2.79 (90) (1 0 1)	2.06 (34) (2 2 0)	2.02 (74) (2 1 1)	1.48 (23) (1 1 2)	
SnO[a]	3.39 (100)	3.00 (50)	2.89 (90)	2.67 (90)	1.77 (80)	
SnO_2[a]	3.35 (100) (1 1 0)	2.64 (80) (1 0 1)	2.37 (25) (2 0 0)	1.77 (65) (2 1 1)	1.68 (18) (2 2 0)	
SnS[a]	3.24 (15) (0 2 1)	2.83 (25) (1 1 1)	2.79 (100) (0 4 0)	2.31 (15) (1 3 1)	1.40 (70) (1 7 1)	
SnS_2[a]	3.15 (40) (1 0 0)	2.78 (100) (1 0 1)	2.14 (50) (1 0 2)	1.82 (50) (1 1 0)	1.74 (32) (1 0 0)	
In air atmosphere						
Me_2Sn(L-**1**)$_2$	2.81 (100)	2.64 (12)	–	1.76 (7)	1.63 (15)	49.95
n-Bu_2Sn(L-**1**)$_2$	3.35 (100)	2.64 (90)	2.37 (37)	1.76 (55)	1.67 (55)	23.45
Ph_2Sn(L-**1**)$_2$	3.34 (100)	2.63 (81)	2.33 (45)	1.76 (38)	1.63 (34)	18.28
Me_3Sn(L-**1**)	3.34 (100)	2.63 (72)	2.35 (48)	1.76 (46)	–	15.26
Ph_3Sn(L-**1**)	3.34 (100)	2.64 (78)	2.31 (36)	1.76 (60)	1.67 (33)	12.27
Me_2Sn(L-**2**)$_2$	3.34 (9) –	2.64 (12) 3.11 (7)	– 2.81 (100)	1.76 (5) –	1.62 (19)	35.41
n-Bu_2Sn(L-**2**)$_2$	3.33 (100)	2.64 (68)	2.37 (33)	1.76 (34)	1.68 (24)	44.45
Me_3Sn(L-**2**)	3.35 (100)	2.64 (95)	2.37 (31)	1.76 (74)	1.67 (24)	19.64
Ph_3Sn(L-**2**)	3.34 (97)	2.64 (100)	2.37 (38)	1.76 (77)	1.67 (29)	23.46
In nitrogen atmosphere						
Me_2Sn(L-**1**)$_2$	3.27 (92)	2.87 (73)	2.81 (83)	2.16 (73)	1.44 (77)	–
n-Bu_2Sn(L-**1**)$_2$	3.16 (44)	2.83 (47)	–	2.17 (34)	1.47 (18)	35.40
Ph_2Sn(L-**1**)$_2$	3.26 (27)	2.83 (100)	–	2.31 (28)	1.41 (12)	29.30
Me_3Sn(L-**1**)	–	2.89 (–)	2.48 (–)	2.06 (–)	1.46 (–)	15.84
Ph_3Sn(L-**1**)	3.20 (88)	–	2.75 (81)	2.31 (56)	1.47 (33)	27.65
Me_2Sn(L-**2**)$_2$	3.25 (11) 2.91 (3)	2.81 (100) –	– –	1.99 (59) –	1.41 (9)	26.54
n-Bu_2Sn(L-**2**)$_2$	3.17 (36)	–	2.78 (44)	2.36 (27)	1.41 (21)	22.40
Me_3Sn(L-**2**)	3.26 (29)	2.82 (100)	–	2.31 (10)	1.41 (11)	29.29
Ph_3Sn(L-**2**)	3.23 (45)	2.82 (100)	–	2.24 (16)	1.41 (13)	29.30

[a] Ref. [32].

and followed by the continuous sublimation of the residue up to 995 °C leaving only 7% residue at 995 °C. The observed d values in the XRD spectrum of the residue obtained at ~995 °C indicated the formation of SnS (Table 5).

In air and nitrogen, *n*-Bu_2Sn(L-**2**)$_2$ decomposed in two and three steps, respectively. In both air and nitrogen, the loss of N_2H_4 occurred in the first step. Further, in air atmosphere, all the organic moieties are lost along with oxidation of tin in the second step, leaving a residue of 25.80% (calcd. for SnO_2: 29.02%) at 560 °C, which has been confirmed as SnO_2 by its XRD data (Table 5). In nitrogen, the mass loss observed (62.70%) in the second step corresponds to the loss of rest of organic moiety (calcd.: 64.82%). The residue obtained at 490 °C has been confirmed as SnS by its XRD spectrum, which sublimed on further heating up to 995 °C leaving 3.9% residue.

In air, a four step decomposition mechanism is proposed for Ph_2Sn(L-**1**)$_2$ on the basis of its DTG curve. For the first two decomposition steps, the loss of N_2H_4 and C_2H_6 are tentatively proposed. The mass loss observed in the third step corresponds to the loss of one triazole ring moiety, which is followed by the loss of rest of the organic moieties with simultaneous oxidation of tin (Table 1). The residue left (obsd. 24.09%; calcd. for SnO_2: 28.01%) at ~600 °C has been confirmed as SnO_2 by its XRD spectrum. However, in nitrogen, the decomposition of Ph_2Sn(L-**1**)$_2$ occurred in two steps. In the first step, all organic moieties are lost, followed by a slow decomposition step in the temperature range 323–725 °C. The XRD analysis of the residue left (27.0%) at 725 °C suggests SnS as end product.

3.3. Thermal decomposition of triorganotin(IV) triazolates under air and nitrogen

Both in air and nitrogen, the thermal decomposition of Me_3Sn(L-**1**) occurred in three steps. The weight loss observed in first step corresponds to the loss of ligand moiety in both the atmospheres. Thereafter, a loss of $3CH_3 + S$ (i.e. C_3H_9S) and $3CH_3$ occurred in air and nitrogen, respectively. The XRD analyses of the residues obtained at 300 °C suggested the formation of a mixture of SnO_2 and Sn in air, and of SnS + Sn in nitrogen [32]. On further heating, up to ~1000 °C an unexpected mass loss step was observed in both the atmospheres, which might be due to the sublimation of the residue.

In air and nitrogen, the decomposition of Me_3Sn(L-**2**) occurred in four and three steps, respectively, with unexpectedly high aggregate mass loss (obsd.: 81.60% in air, 96.60% in nitrogen; calculated mass loss on considering Sn as final residue: 61.33%). The mass losses observed for the first two steps correspond to the loss of NH_2 and rest of the ligand moiety along with methyl groups attached to tin, respectively, in both air and nitrogen. Further, in air the intermediate is oxidized which is evidenced by an exothermic peak at 593 °C in DTA curve (Table 3). Thereafter, in air and nitrogen an unexpected mass loss was observed (Tables 3 and 4) which might

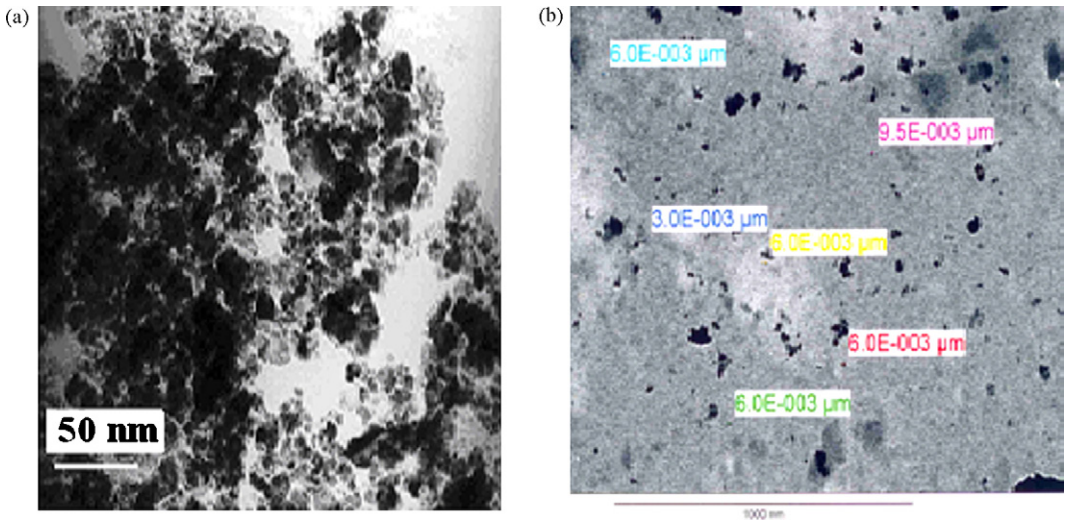

Fig. 7. TEM image of residues obtained by thermal decomposition of *n*-$Bu_2Sn(L\text{-}\mathbf{1})_2$ in nitrogen (a); *n*-$Bu_2Sn(L\text{-}\mathbf{2})_2$ in air (b).

be due to the sublimation of the residue. The main diffraction lines observed in the XRD pattern of the residues, obtained at ~600 °C are found to correspond to those of SnO_2 in air and a mixture of SnS + Sn in nitrogen [32].

In air, the decomposition of $Ph_3Sn(L\text{-}\mathbf{1})$ occurred in a single step and the experimental mass loss corresponds to the loss of all organic moieties along with oxidation of tin, which is evidenced by exothermic peaks at 365 and 512 °C observed in its DTA curve. The XRD pattern of the residue obtained at ~540 °C is indicative of the formation of SnO_2 [32]. Whereas, in nitrogen, it decomposes in two steps, and the first mass loss step corresponds to the loss of most of organic moieties. The XRD analysis of the residue suggested the formation of a mixture of SnS + Sn at 370 °C which sublimed continuously up to 760 °C without leaving any residue.

$Ph_3Sn(L\text{-}\mathbf{2})$ decomposed in three steps in both air and nitrogen. The first two steps are identical in both atmospheres and correspond to the loss of C_2H_7N and $C_{20}H_{15}N_3$, respectively. The simultaneous oxidation also occurred in air which was evidenced by some additional peaks in DTA at 254, 308 and 346 °C. Further, in air, the third weight loss step occurred in the temperature range 418–660 °C, which corresponds to oxidation (Table 3) leaving a residue of 28.0% (calcd. for SnO_2: 30.40%). The XRD analysis of the white powder showed the formation of SnO_2. However, the XRD analysis of the black–grey powder obtained at 452 °C in nitrogen confirmed it as SnS, which sublimed continuously up to 993 °C (Fig. 2).

3.4. Surface morphology and size determination of the residue (SnO_2/SnS)

The crystallite average size of the residues obtained by the pyrolysis of the R_2SnL_2/R_3SnL (in air/nitrogen) has been calculated by using Scherrer equation [2], and the values are in the range ~12 to 50 nm (Table 5).

The SEM images of only those residues, which have been characterized as pure SnO_2 and SnS by powder XRD, are recorded. A few SEM images of the residues obtained by thermal decomposition of $Ph_3Sn(L\text{-}\mathbf{1})$ and *n*-$Bu_2Sn(L\text{-}\mathbf{2})_2$ in air, and *n*-$Bu_2Sn(L\text{-}\mathbf{1})_2$ and $Ph_3Sn(L\text{-}\mathbf{2})$ in nitrogen are shown in Fig. 6 (a)–(d). The SEM images show that the shape of the grain is nearly spherical with almost uniform grain boundary. The measured grain size of the residue obtained by pyrolysis of $Ph_3Sn(L\text{-}\mathbf{1})$ and *n*-$Bu_2Sn(L\text{-}\mathbf{2})_2$ in air, and *n*-$Bu_2Sn(L\text{-}\mathbf{1})_2$ and $Ph_3Sn(L\text{-}\mathbf{2})$ in nitrogen is in the range of ~60 to 105 nm. Due to poor resolution of the images at high magnification value, it is very difficult to measure the smallest particles present in the sample.

The size of the grains of the residues obtained by pyrolysis of *n*-$Bu_2Sn(L\text{-}\mathbf{1})_2$ in nitrogen, and *n*-$Bu_2Sn(L\text{-}\mathbf{2})_2$ in air, is also measured by TEM (Fig. 7(a) and (b), respectively). The size determined by TEM is in the range of ~6.0 to 60.0 nm.

4. Conclusions

Di- and triorganotin(IV) triazolates pyrolyzed under different modes yielding SnO_2 and SnS (or SnS + Sn) in air and nitrogen atmospheres, respectively, as final residue. Thermal decomposition behavior along with SEM, TEM and XRD studies indicated that $Ph_2Sn(L\text{-}\mathbf{1})_2$ is the best precursor for production of pure-phase nanoscale SnO_2 and *n*-$Bu_2Sn(L\text{-}2)_2$ for SnS among the studied precursors, however, *n*-$Bu_2Sn(L\text{-}\mathbf{1})_2$ is found to be a better precursor for the production of both nanoscale pure-phase SnO_2 and SnS.

Acknowledgements

The authors are thankful to the Heads, Department of Metallurgy and Material Science and Institute Instrumentation Center, Indian Institute of Technology Roorkee, Roorkee, and to the Head, Electron Microscopic Section, All India Institute of Medical Science, New Delhi. Ms. Sulaxna is also grateful to the Council of Scientific and Industrial Research, New Delhi, for awarding Senior Research Fellowship.

References

[1] G.A. Costa, M.C. Silva, A.C.B. Silva, G.M. de Lima, R.M. Lago, M.T.C. Sansiviero, Phys. Chem. Chem. Phys. 2 (2000) 5708–5711 (references therein).
[2] A.G. Pereira, L.A.R. Batalha, A.O. Porto, G.M. de Lima, G.G. Silva, J.D. Ardisson, H.G.L. Siebald, Mater. Res. Bull. 38 (2003) 1805–1817.
[3] M. Nath, Sulaxna, Mater. Res. Bull. 41 (2006) 78–91.
[4] L.Y. Zhu, G. Yu, X.Q. Wang, X.Q. Hou, X.J. Liu, J. Sun, Z.H. Sun, H.L. Fan, D. Xu, Thermochim. Acta 473 (2008) 81–85.
[5] M. Nath, Sulaxna, Indian J. Chem. 47A (2008) 510–516.
[6] C.G.R. Nair, S. Mathew, K.N. Ninan, J. Therm. Anal. 37 (1991) 2325–2334.
[7] Y. Deutsch, Y. Natham, S. Sarig, J. Therm. Anal. 42 (1994) 159–174.
[8] S.L. Ali, K. Majid, Thermochim. Acta 311 (1998) 173–181.
[9] N. Petrova, D. Todorovsky, Mater. Res. Bull. 41 (2006) 576–589.
[10] J.B. Johnoson, H. Jones, B.S. Lathan, J.D. Parker, R.D. Engelken, C. Barber, Semicond. Sci. Technol. 14 (1999) 501–507.
[11] S.C. Ray, M.K. Karanjai, Dasgupta, Thin Solid Films 350 (1999) 72–78.
[12] I. Yagi, S. Kavenko, Chem. Lett. 21 (1992) 2345–2348.
[13] I. Yagi, E. Ikeda, Y. Kuniya, J. Mater. Res. 9 (1994) 663–668.
[14] J. Kaur, S.C. Roy, M.C. Bhatnagar, Sens. Actuators B 123 (2007) 1090–1095.

[15] M. Kojima, F. Takahashi, K. Kinoshita, T. Nishibe, M. Ichidate, Thin Solid Films 392 (2001) 349–354.
[16] A. Mosquera, J.E. Rodríguez-Páez, J.A. Varela, P.R. Bueno, J. Eur. Ceram. Soc. 27 (2007) 3893–3896.
[17] M.R. Cássia-Santos, V.C. Sousa, M.M. Oliveira, F.R. Sensato, W.K. Bacelar, J.W. Gomes, E. Longo, E.R. Leite, J.A. Varela, Mater. Chem. Phys. 90 (2005) 1–9.
[18] S. Schlecht, L. Kienle, Inorg. Chem. 40 (2001) 5719–5721.
[19] H. Hu, B. Yang, J. Zeng, Y. Qian, Mater. Chem. Phys. 86 (2004) 233–237.
[20] G.Z. Shen, D. Shen, K.B. Tang, L.Y. Huang, Y.T. Qian, G.E. Zhou, Inorg. Chem. Commun. 6 (2003) 178–180.
[21] D. Chen, G.Z. Shen, K.B. Tang, S.Z. Lei, H.G. Zheng, Y.T. Qian, J. Cryst. Growth 260 (2004) 469–474.
[22] Y.K. Liu, D.D. Hou, G.H. Wang, Chem. Phys. Lett. 379 (2003) 67–73.
[23] M.M. Rao, M. Jayalakshmi, R.S. Reddy, Chem. Lett. 33 (2004) 1044–1045.
[24] X.-L. Gou, J. Chen, P.-W. Shen, Mater. Chem. Phys. 93 (2005) 557–566 (references therein).
[25] J.-J. Zhu, J.-M. Zhu, X.-H. Liao, J.-L. Fang, M.-G. Zhou, H.-Y. Chen, Mater. Lett. 53 (2002) 12–19.
[26] A.G. Pereira, A.O. Porto, G.G. Silva, G.M. de Lima, H.G.L. Siebald, J.L. Neto, Phys. Chem. Chem. Phys. 4 (2002) 4528–4532.
[27] L. Vayssieres, M. Graetzel, Angew. Chem. Int. Ed. 43 (2004) 3666–3670.
[28] M. Nath, Sulaxna, G. Eng, X. Song, Spectrochem. Acta Part A 64 (2006) 148–155.
[29] M. Nath, Sulaxna, X. Song, G. Eng, J. Organomet. Chem. 691 (2006) 1649–1657.
[30] M. Nath, P.K. Saini, G. Eng, X. Song, J. Organomet. Chem. 693 (2008) 2271–2278.
[31] M. Nath, Sulaxna, X. Song, G. Eng, A. Kumar, Spectrochim. Acta Part A 70 (2008) 766–774.
[32] Powder Diffraction File, Sets 1–10, Joint Committee on Powder Diffraction Standards, Philadelphia, PA, 1967, pp. 213, 546.